Inorganic Chemistry
Article

Inorg. Chem. **2010**, *49*, 427–434 **427**
DOI: 10.1021/ic901216g

Crystal Structure and Magnetism of a Well Isolated 2D-Quantum Heisenberg Antiferromagnet, (Quinolinium)$_2$CuBr$_4$·2H$_2$O, and Its Anhydrous Form

Robert T. Butcher and Mark M. Turnbull*

Carlson School of Chemistry and Biochemistry, Clark University, 950 Main Street, Worcester, Massachusetts 01610

Christopher P. Landee, Alex Shapiro, and Fan Xiao

Department of Physics, Clark University, 950 Main Street, Worcester, Massachusetts 01610

David Garrett and Ward T. Robinson

Department of Chemistry, University of Canterbury, Private Bag 4800, Christchurch, New Zealand

Brendan Twamley

University Research Office, University of Idaho, Moscow, Idaho 83844-3010

Received June 24, 2009

Reaction of quinoline with HBr and $CuBr_2$ generates a mixture of two compounds, (quinolinium)$_2$CuBr$_4$·2H$_2$O (**1**) and (quinolinium)$_2$CuBr$_4$ (**2**) for which single-crystal X-ray structures have been solved. Compound **1** crystallizes in the monoclinic space group $C2/c$ as layers of tetrabromocuprate ions which are separated by intervening layers of quinolinium ions. Compound **2** crystallizes in the triclinic space group $P\bar{1}$. Magnetic data analysis reveals that **1** behaves as a 2D-quantum Heisenberg antiferromagnet with $2J/k_B = -6.17(3)$ K within the layers. High field magnetization data at low temperatures suggests that T_N must be less than 1.8 K for **1**, yielding a figure of merit $|k_B T_N/2J| < 0.29$, which indicates excellent isolation between the layers. Magnetic exchange in compound **2** was much weaker and was fit to a linear chain antiferromagnet with $2J/k_B = -1.59(3)$ K.

Introduction

Research of 2D layered magnetic systems has been fueled by the discovery of copper oxide-based high T_c superconductors nearly 2 decades ago.[1] The 2D layered structure motif is present in both molecular magnetic insulating materials as well as copper-oxide high T_c superconducting materials. Both insulating and high T_c superconducting materials exhibit antiferromagnetic interactions between four identical nearest neighbors within any particular 2D layer of $S = {}^1/_2$ ions as well as weak antiferromagnetic interactions in a third dimension (between layers). Furthermore, it has been suggested that doped copper oxide systems that become superconducting can be understood in terms of exchange interactions within the layers.[2]

Molecular magnetic complexes of Cu(II) ions possess a d^9 electronic configuration, yielding $S = {}^1/_2$ materials in which it is facile to observe quantum effects. Furthermore, the average g-values are often close to 2, indicating the absence of internal magnetic fields and almost complete quenching of the orbital angular momentum. The resulting magnetic metal−organic complexes of Cu(II) are Heisenberg-like in which the magnetic moments are free to respond to an external field.

Previous examples of molecule-based two-dimensional (2D) $S = {}^1/_2$ Heisenberg antiferromagnet (2D QHAF) systems include the salts (2-amino-5-chloropyridinium)$_2$CuBr$_4$ [(5CAP)$_2$CuBr$_4$][3], (2-amino-5-methylpyridinium)$_2$CuBr$_4$ [(5MAP)$_2$CuBr$_4$][3] and (2-amino-5-bromopyridinium)$_2$CuBr$_4$ [(5BAP)$_2$CuBr$_4$],[4] in which 2D layers are comprised of

*To whom correspondence should be addressed. E-mail: mturnbull@clarku.edu.

(1) For a review, see Kastner, M. A.; Birgeneau, R. J.; Shirane, G.; Endoh, Y. *Rev. Mod. Phys.* **1998**, *70*, 897.
(2) Sokol, A.; Pines, D. *Phys. Rev. Lett.* **1993**, *71*, 2813.
(3) Woodward, F. M.; Albrecht, A. S.; Wynn, C. M.; Landee, C. P. *Phys. Rev. B* **2002**, *65*, 144412.
(4) Woodward, F. M.; Landee, C. P.; Giantsidis, J.; Turnbull, M. M.; Richardson, C. *Inorg. Chim. Acta* **2001**, *324*, 324.

Published on Web 12/16/2009

tetrabromocuprate ions, although the layers are not well isolated due to close Br···Br distances between the layers. Other quasi-2D QHAF systems in which both the magnetism and structure have been published are limited.[5] Examples of pyrazine-bridged 2D layered metal−organic complexes include $[Cu(pyrazine)_2](ClO_4)_2$, $[Cu(pyrazine)_2](BF_4)_2$, and $[Cu(pyrazine)_2(NO_3)](PF_6)$,[6] $[Cu(pyrazine)_2(HF_2)]BF_4$,[7] $[Cu(pyrazine)_2(NO_2)](ClO_4)$,[8] and $Cu(pyrazine)_2V_6O_{16}\cdot(H_2O)_{0.22}$.[9] However, metal−organic 2D QHAF systems are always limited due to the presence of interactions in a third dimension that occur between layers, albeit small.

Our research interests require a library of 2D QHAF systems in which to explore both magnetic susceptibility and field dependent magnetization behavior. Exchange strengths derived from susceptibility data are fairly common, although experimental results regarding field dependent data remain largely unexplored. A relatively weak antiferromagnetic exchange within the layers implies that an external field can drive the system to saturation in which the magnetic moments in the sample are aligned with the applied field. The Hamiltonian is used in this work where an antiferromagnetic interaction is represented by a negative value of J. $H = -2J\sum_{nn} S_i \cdot S_{i+1}$. In contrast, superconducting copper oxide systems have exchange strengths on the order of $|2J/k| \sim 1500$ K[10] that require unrealistic applied magnetic fields to reach saturation. Fortunately, molecular magnetic systems that have exchange strengths on the order of $2J/k_B \sim 5-10$ K such as $[(5CAP)_2CuBr_4]$,[11] $[(5MAP)_2CuBr_4]$[3], and $[(5BAP)_2CuBr_4]$ have saturation moments that are accessible in an applied field of ~33 T. Here, we report the synthesis, structure, and magnetic behavior of the two-dimensional $S = {}^1/_2$ Heisenberg antiferromagnet $(quinolinium)_2CuBr_4\cdot 2H_2O$ (**1**) and its anhydrous analogue $(quinolinium)_2CuBr_4$ (**2**).

Experimental Section

HBr(aq) and quinoline were purchased from Aldrich Chemical Co., while Cu(II) bromide was purchased from Aesar Chemical Company. All chemicals were used as received. Infrared (IR) spectra were recorded on a Perkin-Elmer Paragon 500 spectrophotometer as KBr pellets or on a Smiths Detection IlluminatIR system via attenuated total reflectance (ATR) as single crystals.

Synthesis

$(Quinolinium)_2CuBr_4\cdot 2H_2O$ (1). Quinoline (2.603 g, 20.2 mmol) was dissolved in 40 mL of 2.0 M HBr yielding a light yellow solution. $CuBr_2$ (2.234 g, 10.0 mmol) was added to the stirred mixture yielding a light green solution. The acidic mixture was filtered and allowed to slowly evaporate for 5 days in an open plastic beaker. The resulting nearly opaque black blocks were recovered by filtration, washed with *t*-BuOH, and stored in a humid environment to prevent loss of water. Recovered 0.561 g (33%). IR (ATR) ν 3436 br, m O−H ν, 2400 m, 1634 m, 1593 m O−H δ, 1556 s, 1485 w, 1404 w, 1379 w, 1300 m, 1222 m, 1157 w, 1129 w, 988 w, 939 w, 910 w, 859 w, 801 s, 765 s cm^{-1}. Powder X-ray diffraction (XRD) was performed and compared to the X-ray lattice paramenters of **1** to verify that the materials were of the same phase.

$(Quinolinium)_2CuBr_4$ (2). Single crystals were obtained through the synthesis above and were observed as translucent laths mixed with crystals of **1** and isolated mechanically under a stereomicroscope. Yield: <1%. A larger sample of **2** was prepared by placing a sample of **1** in an oven for 1 h at 150 °C to remove the waters of hydration. The conversion of **1** to **2** by this method is quantitative. The material was subsequently stored in a desiccator. IR (KBr) ν 2618 m, 1636 s, 1595 s, 1558 s, 1376.3 m, 1301 m, 1334 m, 939 w, 804 s, 769 s, 611 m, 520 w, 472 m cm^{-1}. Powder XRD was performed and compared to the X-ray lattice parameters of **2** to verify that the materials were of the same phase.

X-ray Structures. Crystals of compound **1** were removed from the flask and covered with a layer of hydrocarbon oil to prevent loss of water. A suitable crystal was selected, attached to a glass fiber, and placed in the low-temperature nitrogen stream.[12] A suitable crystal of **2** was taken directly from the product mixture and treated normally. Data for **1** and **2** were collected at 87(2) K and 130 (2) K, respectively, using a Bruker/Siemens SMART APEX instrument (Mo Kα radiation, λ = 0.710 73 Å) equipped with a Cryocool NeverIce low temperature device. Data were measured using omega scans of 0.3° per frame for 30 s, and a full sphere of data was collected. A total of 2450 frames were collected. The first 50 frames were recollected at the end of data collection to monitor for decay. No decomposition was observed. Cell parameters were retrieved using SMART[13] software and refined using SAINTPlus[14] on all observed reflections. Data reduction and correction for Lp and decay were performed using the SAINTPlus software. Absorption corrections were applied using SADABS.[15] The structure was solved by direct methods and refined by least-squares method on F^2 using the SHELXTL program package.[16] All non-hydrogen atoms

(5) (a) Greven, M.; Birgeneau, R.; Endoh, Y.; Kastner, M.; Matsuda, M.; Shirane, G. *Z. Phys B: Condens. Matter* **1995**, *96*, 465. (b) Ronnow, J. M.; McMorrow, D. F.; Harrions, A. *Phys. Rev. Lett.* **1999**, *83*, 3152. (c) Yamagata, K.; Abe, H. *J. Magn. Magn. Mater.* **1983**, *31−34*, 1179. (d) Koyama, K.; Nobumasa, H.; Matsura, M. *J. Phys. Soc. Jpn.* **1987**, *56*, 1553. (e) Heñido, Y.; Yamada, K.; Birgeneau, R. J.; Gabbe, D. R.; Jenssen, H. P.; Kastner, M. A.; Peters, C. J.; Picote, P. J.; Thurston, T. R.; Tranquada, J. M.; Shirane, G.; Hidaka, T.; Oda, M.; Enomoto, Y.; Suzuki, M.; Murakami, T. *Phys. Rev. B* **1988**, *37*, 7443. (f) Algra, H.; de Jongh, L.; Carlin, R. *Physica B+C* **1978**, *93B*, 24. (g) Lumsden, M. D.; Sales, B. C.; Mandrus, D.; Nagler, S. E.; Thompson, J. R. *Phys. Rev. Lett.* **2001**, *86*, 159.
(6) Woodward, M. F.; Gibson, P. J.; Jameson, G. B.; Landee, C. P.; Turnbull, M. M.; Willett, R. D. *Inorg. Chem.* **2007**, *46*, 4256.
(7) (a) Manson, J. L.; Conner, M. M.; Schlueter, J. A.; Hyzer, K. A. *Polyhedron* **2007**, *26*, 1912–1916. (b) Middlemiss, D. S.; Lawton, L. M.; Morrison, C. A.; Wilson, C. C. *Chem. Phys. Lett.* **2008**, *459*, 119–123. (c) Lancaster, T.; Blundell, S. J.; Baker, P. J.; Brooks, M. L.; Hayes, W.; Pratt, F. L.; Manson, J. L.; Conner, M. M.; Schlueter, J. A. *Phys. Rev. Lett.* **2007**, *99*, 267601/1–267601/4.
(8) Liu, T.; Chen, Y.-H.; Zhang, Y.-J.; Wang, Z.-M.; Gao, S. *Inorg. Chem.* **2006**, *45*, 9148.
(9) Maggard, P. A.; Boyle, P. D. *Inorg. Chem.* **2003**, *42*, 4250–52.
(10) Birgeneau, R. *Am. J. Phys.* **1990**, *58*, 28.
(11) Woodward, F. M.; Albrecht, A. S.; Wynn, C. M.; Landee, C. P. *Phys Rev. B* **2002**, *65*, 144412.
(12) Hope, H. *Prog. Inorg. Chem.* **1994**, *41*, 1.
(13) *SMART*, version 5.626, Bruker Molecular Analysis Research Tool; Bruker AXS: Madison, WI, **2002**.
(14) *SAINTPlus*, version 6.45a, Data Reduction and Correction Program; Bruker AXS: Madison, WI, 2003.
(15) *SADABS*, version 2.01, an empirical absorption correction program; Bruker AXS Inc.: Madison, WI, 2004.
(16) *SHELXTL*, version 6.10, Structure Determination Software Suite; Sheldrick, G. M., Bruker AXS Inc.: Madison, WI, 2001.

Table 1. Crystal and Structure Refinement Data for **1** and **2**

empirical formula	$C_{18}H_{20}N_2O_2CuBr_4$	$C_{18}H_{16}N_2CuBr_4$
formula weight	679.54	643.51
temperature	87(2) K	150(2) K
wavelength	0.710 73 Å	0.710 73 Å
crystal system	monoclinic	triclinic
space group	$C2/c$	$P\bar{1}$
unit cell dimensions	a = 12.3323(7) Å	a = 7.6738(2) Å
	b = 9.7972(6) Å	b = 8.9490(2) Å
	c = 18.6504(11) Å	c = 16.325(5) Å
	α = 90°	α = 78.711(1)°.
	β = 100.3220(10)°	β = 83.454(1)°.
	γ = 90°	γ = 71.745(1)°.
volume	2216.9(2) Å^3	1042.42(5) Å^3
Z	4	2
density (calculated)	2.036 Mg/m^3	2.050 Mg/m^3
absorption coefficient	8.210 mm^{-1}	8.717 mm^{-1}
F(000)	1308	614
crystal size	0.42 × 0.26 × 0.18 mm^3	0.63 × 0.16 × 0.07 mm^3
θ range for data collection	2.22 to 25.25°	2.55 to 26.37°
index ranges	$-14 \le h \le 14$, $-11 \le k \le 11$, $-22 \le l \le 22$	$-9 \le h \le 9$, $-11 \le k \le 11$, $-20 \le l \le 20$
reflections collected	11 958	12 194
independent reflections	2013 [R(int) = 0.0256]	4241 [R(int) = 0.0240]
completeness to θ = 25.25°	99.90%	99.6%
refinement method	full-matrix least-squares on F^2	full-matrix least-squares on F^2
data/restraints/parameters	2013/0/163	4241/0/232
goodness of fit on F^2	1.061	1.033
final R indices [$I > 2\sigma(I)$]	R1 = 0.0246, wR2 = 0.0611	R1 = 0.0235, wR2 = 0.0567
R indices (all data)	R1 = 0.0261, wR2 = 0.0618	R1 = 0.0284, wR2 = 0.0592
largest diff. peak and hole	2.076 (near Br1) and −0.603 e/Å^3	0.697 and −1.250 (near Br1) e/Å^3

were refined anisotropically. Hydrogen atoms were located in the Fourier map and their positions refined with fixed isotropic thermal parameters. Details of the data collection and refinement are given in Table 1. Further details are provided in the Supporting Information.

Magnetic Measurements. Magnetic susceptibility data were collected using a Quantum Design MPMS-XL SQUID magnetometer. For both compounds, the first study was an isothermal magnetization at 1.8 K in fields up to 5 T. For each compound, the magnetization was linear with field up to 1 T and no hysteresis was observed. Temperature-dependent magnetization was collected for both compounds in fields of 0.1 T and was converted to susceptibility data using a diamagnetic correction of -3.33×10^{-4} and TIP of 6×10^{-5}. Prior to loading the sample of **1** into the SQUID, a crystalline sample was kept in a cool humid environment overnight. Grinding the sample of **1** was not performed and the sample was loaded into the SQUID at 290 K to avoid dehydration. The high-field magnetization of sample **1** was measured using a vibrating sample magnetometer at 4.3 K in fields up to 33 T at the National High Magnetic Field Laboratory in Tallahassee, Florida. The sample was kept in an sealed container until the experimental study but became damp in the humid atmosphere during the loading procedure. EPR experiments were performed at two different frequencies, X-band and Q-band, which correspond to a ν of approximately 9.8 and 34 GHz and $h\nu$ of about 0.3 and 1.1 cm^{-1} (0.4 and 1.6 K), respectively.

A crystalline sample of **2** was ground into a powder and heated in an oven at 150 °C for an hour. The sample was then packed into a gelcap in a drybox and placed into a straw. The sample was stored in a desiccator until it was placed into the SQUID magnetometer, where it was held at 53 °C for 10 min and purged many times with He gas to ensure that the sample was anhydrous.

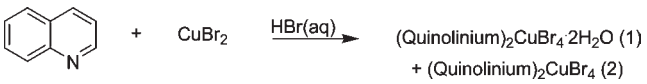

Figure 1. Reaction of quinoline with copper(II) bromide in aqueous HBr.

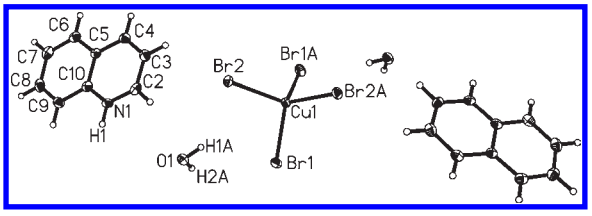

Figure 2. Asymmetric unit of 1. Hydrogen atoms are drawn as spheres of arbitrary size, while all other atoms are shown as thermal ellipsoids at 50% probability. Only the asymmetric unit and copper coordination sphere are labeled.

Results

Synthesis and Structure. Single crystals of **1** and **2** suitable for X-ray diffraction were grown by slow evaporation from aqueous acidic solution (Figure 1). The two materials can be readily interconverted by either warming to remove the waters of hydration or by storing the sample in a humid environment. Powder X-ray diffraction was used to verify the identities of the samples.

Compound **1** crystallizes in the monoclinic space group $C2/c$, with unit cell parameters a = 12.3323(7) Å, b = 9.7972(6) Å, c = 18.6504(11) Å, and β = 100.322(1)°. The molecular unit is shown in Figure 2. The structure refinement data are given in Table 1, with bond lengths and angles in Table 2. Hydrogen bond data are given in Table 3.

The symmetry of the $CuBr_4^{2-}$ tetrahedron is reduced toward square planar geometry due to the Jahn−Teller distortion, yielding C_2 symmetry, as is common in Cu(II)

Table 2. Bond Lengths [Å] and Angles [deg] for **1** and **2**[a]

bond	cmpd **1**	cmpd **2**	angle	cmpd **1**	cmpd **2**
Cu(1)−Br(1)	2.3469(4)	2.3862(5)	Br(1)−Cu(1)−Br(2)	100.677(11)	99.080(15)
Cu(1)−Br(2)	2.4118(4)	2.3972(4)	Br(1)−Cu(1)−Br(1)A	127.18(3)	
Cu(1)−Br(3)		2.3847(4)	Br(1)no. 1−Cu(1)−Br(2)	104.702(11)	
Cu(1)−Br(4)		2.3940(4)	Br(2)−Cu(1)−Br(2)A	120.85(3)	
			Br(3)−Cu(1)−Br(4)		99.165(15)
			Br(3)−Cu(1)−Br(2)		132.617(19)
			Br(3)−Cu(1)−Br(1)		99.896(16)
			Br(1)−Cu(1)−Br(4)		131.292(19)
			Br(4)−Cu(1)−Br(2)		100.010(15)

[a] Symmetry transformations used to generate equivalent atoms: $A = -x, y, -z + {}^1/_2$.

Table 3. Hydrogen Bonds for 1 [Å and deg][a]

D−H···A	*d*(D−H)	*d*(H···A)	*D*(D···A)	angle (DHA)
		Compound **1**		
O(1)−H(1A)···Br(2)	0.75(6)	2.88(6)	3.488(3)	141(5)
O(1)−H(1A)···Br(1)	0.75(6)	2.99(6)	3.574(3)	137(5)
O(1)−H(1B)···Br(2)no. 1	0.74(5)	2.60(5)	3.330(3)	169(5)
N(1)−H(1)···O(1)no. 2	0.79(4)	1.96(4)	2.748(4)	174(4)
		Compound **2**		
N(1)−H(1)···Br(3)	0.84(3)	2.54(3)	3.347(2)	161(3)
N(11)−H(11)···Br(2)no. 3	0.93(3)	2.39(3)	3.303(2)	166(2)

[a] Symmetry transformations used to generate equivalent atoms: no. 1, $-x + {}^1/_2, y - {}^1/_2, -z + {}^1/_2$; no. 2, $-x + 1, y, -z + {}^1/_2$; no. 3, $-x + 2, -y + 1, -z + 1$.

tetrahedral complexes.[17] The degree of distortion can be described structurally as the mean trans angle (mta), which is the average of the two enlarged Br−Cu−Br angles. For **1**, the mta value of 124.0° is significantly closer to an idealized tetrahedral than square planar. The mta is small in comparison to other tetrabromocuprate compounds, such as (pyridinium)$_2$CuBr$_4$[18] (mta = 131.3°), (ethylendiammonium)CuBr$_4$[19] (mta = 180°), (3-ammoniumpyridinium)CuBr$_4$[20] (mta = 170.5°), and (2-amino-5-bromopyridinium)$_2$ CuBr$_4$[18] (mta = 139°).

There are two unique Cu−Br bonds within each CuBr$_4^{2-}$ ion, the other bromide ions being generated by the C_2 axis through the Cu(II) ion. The Cu−Br bond lengths in **1** (2.3469(4) and 2.4118(4) Å) are similar to those seen in other compounds with smaller mean trans angles, such as (3-ethylpyridinium)$_2$CuBr$_4$[21] (2.373 and 2.388 Å, mta = 130.1°) and (1,2-vinylene(triphenylphosphonium))$_2$CuBr$_4$[22] (2.372 and 2.426 Å, mta = 124.8°).

Waters of hydration are located within layers of CuBr$_4^{2-}$ distorted tetrahedra (Figure 3). The water molecules are hydrogen bonded to quinolinium cations via N−H···O interactions and are also hydrogen bonded to CuBr$_4^{2-}$ anions via O−H···Br interactions. Together, both the N−H···O and O−H···Br hydrogen bonding interactions tie the CuBr$_4^{2-}$ tetrahedra and quinolinium cations together into a layered structure.

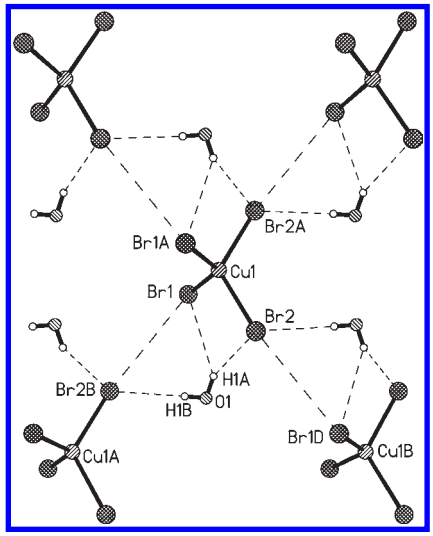

Figure 3. Layers of CuBr$_4^{2-}$ distorted tetrahedra in **1**, viewed perpendicular to the *ab*-plane. Dashed lines illustrate close Br···Br contacts and O−H···Br hydrogen bonds.

Within the *ab*-plane, the CuBr$_4^{2-}$ distorted tetrahedra are related by C-centering. O−H···Br hydrogen bonding forces close Br···Br contacts between corners of CuBr$_4^{2-}$ distorted tetrahedra (Figure 3). The resulting two-halide exchange pathways have 4-fold symmetry between four identical nearest neighbors of CuBr$_4^{2-}$ tetrahedra. The resulting exchange pathways have the parameters $d_{Br1\cdots Br2B}$ = 4.223(2) Å, $\theta_{Cu1-Br1\cdots Br2B} = 122.56(2)°$, $\theta_{Br1\cdots Br2B-Cu1A} = 161.53(3)°$, and $\tau_{Cu1-Br1\cdots Br2B-Cu1A} = 16.00(5)°$.

The crystal packing of **1** shows layers of CuBr$_4$ tetrahedra separated by the quinolinium cations (Figure 4). The quinolinium cations exhibit the normal bond distances and angles in comparison to other quinolinium metal complexes, such as the isomorphous tetrachlorozincate dihydrate analogue (quinolinium)$_2$ZnCl$_2$·2H$_2$O[23] and isomorphous tetrachlorocuprate dihydrate (quinolinium)$_2$CuCl$_4$·2H$_2$O.[24]

The separation of the CuBr$_4^{2-}$ layers can be described by the closest Br···Br distance between them. For compound **1**, the closest Br···Br distance between layers is

(17) Turnbull, M. M.; Landee, C. P.; Wells, B. M. *Coord. Chem. Rev.* **2005**, *249*, 2567.
(18) Luque, A.; Sertucha, J.; Castillo, O.; Roman, P. *New. J. Chem.* **2001**, *25*, 1208.
(19) Halvorson, K.; Willett, R. D. *Acta Crystallogr.* **1988**, *C44*, 2071.
(20) Willett, R. D.; Place, H.; Middleton, M. *J. Am. Chem. Soc.* **1988**, *110*, 8639.
(21) Luque, A.; Sertucha, J.; Castillo, O.; Roman, P. *Polyhedron* **2002**, *21*, 19.
(22) Blachnik, R.; Reuter, H.; Wiest, T.; Eickmeier, H. *Z. Kristallogr.-New Cryst. Struct.* **2000**, *215*, 249.
(23) Valdes-Martinez, J.; Munoz, O.; Toscano, R. A. *Acta Crystallogr., Sect. E: Struct. Rep. Online* **2005**, *61*, m1590.
(24) Lynch, D. E.; McClenaghan, I. *Acta Crystallogr., Sect. E: Struct. Rep. Online* **2002**, *58*, m551.

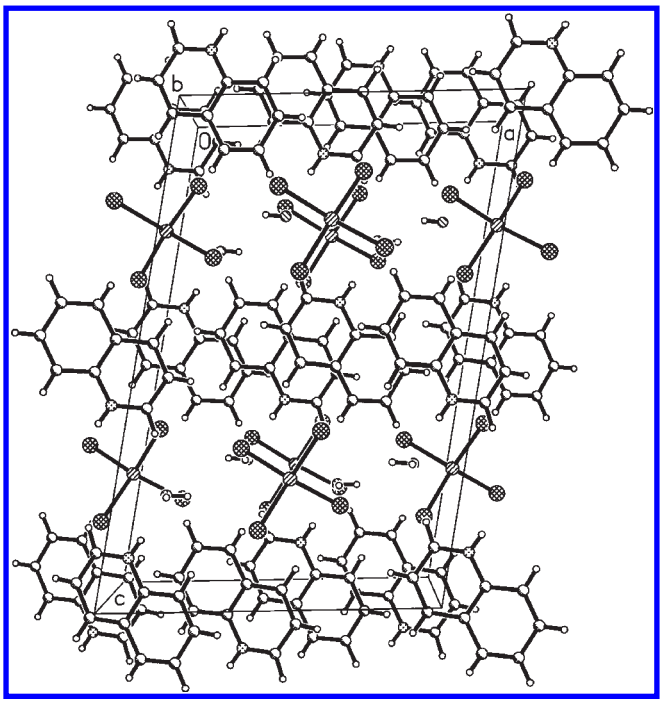

Figure 4. Packing diagram for compound **1** showing the layers of $CuBr_4^{2-}$ dianions separated by quinolinium cations. Hydrogen atoms are drawn as spheres of arbitrary size.

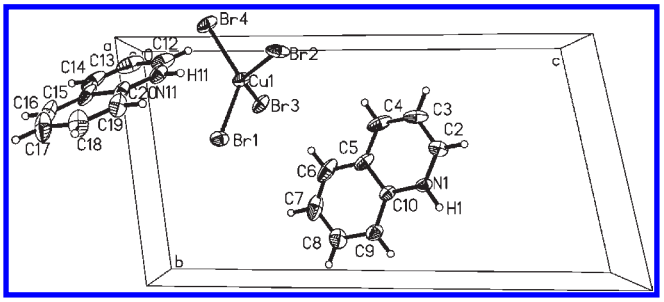

Figure 5. Asymmetric unit in **2** viewed parallel to the *a*-axis. Hydrogens are drawn as spheres of arbitrary size.

5.742 Å. This is a much larger interlayer separation than seen in other 2D copper(II) tetrabromocuprate compounds, such as $(5CAP)_2CuBr_4$ (4.83 Å),[3] $(5MAP)_2CuBr_4$ (4.97 Å),[3] and $(5BAP)_2CuBr_4$ (4.97 Å).[4]

(Quinolinium)$_2$CuBr$_4$. Compound **2** crystallizes in the triclinic space group $P\bar{1}$ with $a = 7.6738(15)$ Å, $b = 8.9490(18)$ Å, $c = 16.3254(3)$ Å, $\alpha = 78.71(3)°$, $\beta = 83.45(3)°$, and $\gamma = 71.74(3)°$. The asymmetric unit is shown in Figure 5. Crystallographic refinement data are given in Table 1, while bond distances and angles are given in Table 2. Hydrogen bond parameters are given in Table 3.

The most obvious difference between the two pseudo-polymorphs is the lack of water molecules in **2**. The lower symmetry of **2** results in four independent Cu−Br bonds of length 2.3847(4), 2.3862(5), 2.3940(4), and 2.3972(9) Å. Again, these bond lengths are in the normal range for tetrabromocuprate compounds, such as in (2,6-diamino-3,5-dibromopyridinium)$_2$ $CuBr_4$ (2.379 and 2.394 Å)[25] and Cu(2-methylpyridinium)$_2CuBr_4$ (2.379 and 2.387 Å).[18]

(25) Willett, R. D.; Haddad, S. F.; Twamley, B. *Acta Crystallogr., Sect. C: Cryst. Struct. Commun.* **2000**, *56*, e437.

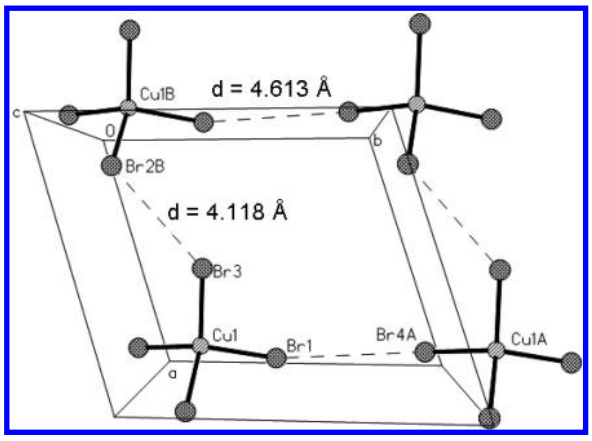

Figure 6. Rectangular magnetic lattice in **2**.

Table 4. Parameters Relevant to Two-Halide Exchange in **1** and **2**

cmpd		d (Å)	θ_1 (deg)	θ_2 (deg)	τ (deg)
1	Cu−Br1···Br2−Cu	4.2228(5)	122.56(1)	161.53(1)	16.00(5)
2	Cu1−Br3···Br2B−Cu1B	4.1180(5)	115.06(1)	137.12(1)	−126.51(2)
2	Cu1−Br1···Br4A−Cu1A	4.6129(4)	150.24(2)	159.81(2)	25.23(4)

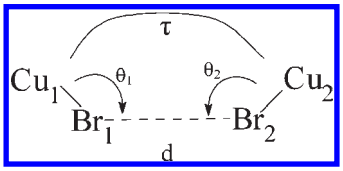

Interestingly, all the Cu−Br bond lengths in **2** are intermediate in length in comparison to the two Cu−Br bond lengths in **1** (2.3470(4) and 2.4118(4) Å). Additionally, the mean trans angle in **2** has increased, relative to **1**, to 131.62°.

Unlike **1**, in which each $CuBr_4^{2-}$ ion interacts with its nearest neighbors via four identical Cu−Br···Br−Cu pathways, each tetrabromocuprate ion in **2** interacts with neighboring $CuBr_4^{2-}$ ions of two unique types. As illustrated in Figure 6, short Br3···Br2B contacts (4.118 Å) form along the *a*-axis. Along the *b*-axis the Br1···Br4A contacts (4.613 Å) are much longer in comparison to those along the *a*-axis and longer than the Br···Br contacts in **1** (4.223 Å). The parameters relevant to the two-halide exchange pathways in **2** are compared with parameters for the two-halide exchange pathway in **1** (Table 4). A review of the relationship between the structural parameters and the magnetic exchange strength is available.[17]

Interestingly, a mixture of the two phases has been observed when the crystals of the dihydrate phase are left at ambient conditions. Attempts to isolate one or the other phase by manual separation under a microscope were not successful due to similarities in color and morphology. However, the pure anhydrous phase **2** can be prepared by heating the sample to ∼150 °C, as characterized by powder X-ray diffraction.

Magnetic Results

Room temperature electron paramagnetic resonance (EPR) spectra were obtained by using a single crystal of **1**. Broad spectra (700G) were observed at room temperature

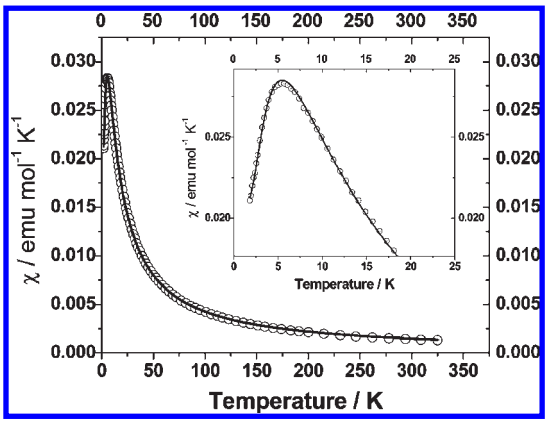

Figure 7. Susceptibility data for **1** and theoretical fit for a 2D layer model (line). Inset shows χ for $0 \leq T \leq 25$ K.

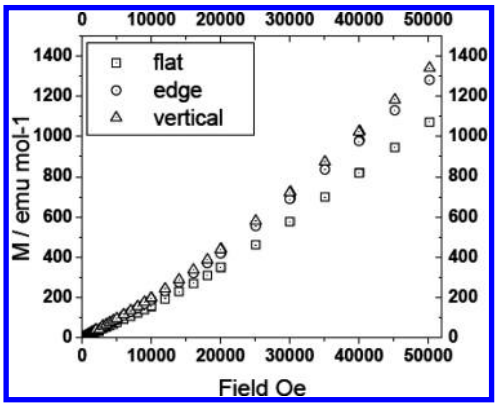

Figure 8. Single crystal magnetization at 1.8 K for **1** with three perpendicular orientations of field.

with a small orientation dependence in g. The line width was reduced to 360G at 77 K with an average g value, $g_{iso} \sim 2.15$, giving a Curie constant of 0.43 ($C = 0.375(g_{iso}/2)^2$).

Magnetic susceptibility data for a polycrystalline sample of **1** show a rounded maximum at ~5.5 K followed by decreasing χ with temperature (Figure 7). Fitting the data to the model for a square magnetic lattice[4] gave $C = 0.448(1)$ emu K mol^{-1} and $2J/k_B = -6.17(3)$ K, with a 0.77(5)% impurity (Figure 7). The quality of the fit is very good, as seen in the insert of Figure 7. The value of C agrees well with that obtained from EPR.

Crystals of **1** grow as flat parallelepipeds. Face indexing showed the c*-axis to be perpendicular to the plates, indicating that the $CuBr_4^{2-}$ layers are oriented parallel to the plate. Single crystal magnetization data at 1.8 K for $0 \leq H \leq 50{,}000$ Oe were collected for **1** with the field oriented in three perpendicular directions, one parallel to the c* axis and the other two within the planes (but not necessarily parallel to the a- or b-axes). There is no evidence of a spin-flop transition along any axis. The data show slight upward curvature for all three crystal directions (Figure 8). The field-dependent magnetizations are nearly identical with the field oriented along two perpendicular directions within the plane of the plate, while the magnetization perpendicular to the plate is significantly smaller (18(2) % difference at 50,000 Oe), indicative of the expected g-factor anisotropy.

High-field magnetization measurements (Figure 9) on polycrystalline samples at 4.3 K for $0 \leq H \leq 33$ T (330 000 Oe) reveal slight upward curvature with increasing field

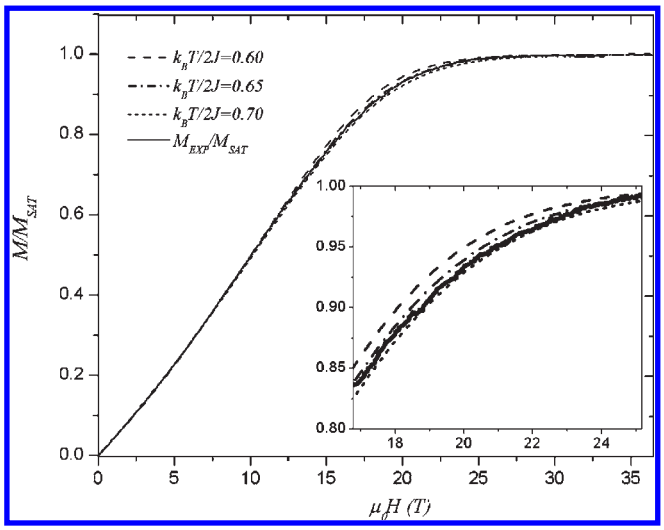

Figure 9. High-field magnetization data for a polycrystalline sample of **1** at 4.3 K and $0 \leq H \leq 33$ T (330 000 Oe). The experimental data is represented by the solid line while the dashed lines correspond to the predicted magnetization curves for a 2D $S = {}^1/_2$ Heisenberg antiferromagnet at different relative ($k_BT/2J$) temperatures.

typical of low-dimensional antiferromagnets, saturation occurring near 20 T. The relatively small saturation field agrees with the observation that the exchange strength within the layers is not strong. The zero-temperature saturation field μ_0H_0 is related to the exchange strength by the molecular-field expression $\mu_0H_0 = zk_B(2|J|)/(g\mu_B)$,[26] in which z is the number of nearest neighbors. For an average g value of 2.15, as determined by EPR, four nearest neighbors, and a $|2J|$ value of 6.17 K, μ_0H_0 is predicted to be 17 T and is found experimentally to be 20 T as shown in Figure 9. At finite temperatures, magnetic excitations reduce the sample's moment and additional fields must be applied to overcome these effects. The extent of rounding of the magnetization data is a function of the ratio of the experimental temperature to the exchange strength, $|k_BT/2J|$. For **1**, $T = 4.3$ K and $2J/k_B = -6.17$ K for a relative temperature of 0.70.

In Figure 9, the experimental data (solid line) are compared to the theoretical predictions for a 2D $S = {}^1/_2$ Heisenberg antiferromagnet at various ratios of $|k_BT/2J|$: 0.70, 0.65, and 0.60 where the ratios $T/2J$ are the relative temperatures and $2J$ is the magnetic exchange within the layers. As seen in the insert, the data most closely follows the theoretical curve for a ratio of 0.65, even though the data are never more than several percent different from the 0.70 curve. The ratio 0.65 corresponds to an exchange strength of $2J/k_B = 4.3$ K/0.65 = 6.6 K, 7% larger than the value obtained from the susceptibility. Considering the unknown effect of the moisture which may have been absorbed by the sample as it was loaded into the instrument, we consider the exchange strength obtained from the magnetization study to be consistent with that of the susceptibility measurement but consider the susceptibility-derived value $2J/k_B = -6.17$ K, corresponding to a saturation field of 17 T, to be more reliable.

No evidence of a field-induced transition was observed in **1** although spin-flop transitions have been observed at ~3000 Oe in $(5CAP)_2CuBr_4$ and 6000 Oe in $(5MAP)_2CuBr_4$,[3] and in a recent series of pyrazine-based 2D $S = {}^1/_2$

(26) Bonner, J. C.; Fisher, M. E. *Phys. Rev.* **1964**, *135*, A640.

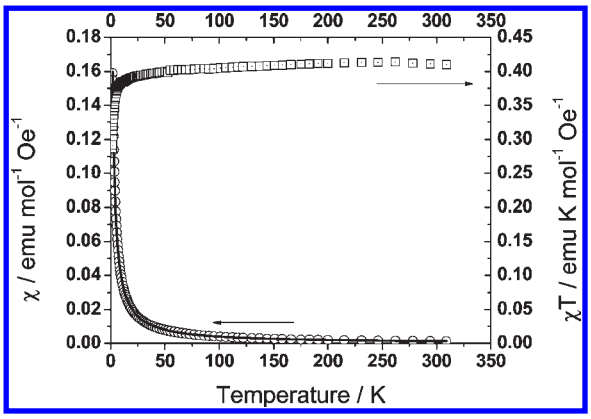

Figure 10. Temperature dependence of χ (○) and χT (□) for **2**. The solid line is the fit to a linear chain model.

Heisenberg antiferromagnets.[27] However, in order to observe a spin-flop transition, the temperature of the sample must be below the ordering transition temperature T_N. The absence of such a transition implies that $T_N < 1.8$ K for **1** and therefore the critical ratio $|k_BT_N/2J| < 0.29$.

The magnetic interactions in **2** are significantly weaker. A plot of χ as a function of temperature does not show a maximum, and χT shows only slight deviation from the Curie law ($\chi T = C$) above ~12 K (Figure 10). The Curie−Weiss constant θ is relatively small at −1.11 K, in agreement with weaker interactions in the sample. The susceptibility for **2** was analyzed according to a linear chain magnetic model[26] which yielded $C = 0.410(1)$ emu K mol^{-1}and $2J/k_B = -1.59(3)$ K (Figure 10).

Discussion

Compound **1** forms layers of $CuBr_4^{2-}$ distorted tetrahedra which are well isolated by layers of quinolinium cations. The $CuBr_4^{2-}$ tetrahedra are related to each other by the *C*-centering, resulting in a square magnetic lattice with each ion having four identical nearest neighbors. Hydrogen bonding to the water molecules in the layer helps to generate close Br···Br contacts between the corners of the $CuBr_4^{2-}$ ions, which provides the superexchange pathway. The fitted magnetic data are in complete agreement with a square magnetic lattice, yielding $2J/k_B = -6.17(3)$ K. The exchange value is similar to that observed in $CuBr_4^{2-}$ compounds with comparable Br···Br separation distances (4.223 Å), such as $(pyridinium)_2CuBr_4$ ($2J/k_B = -4.46$ K, $d = 4.36$ Å),[18] $(5BAP)_2CuBr_4$ ($2J/k_B = -6.94$ K, $d = 4.41$ Å),[4] and $(5CAP)_2CuBr_4$ ($2J/k_B = -8.7$ K, $d = 4.3$ Å).[3]

The interactions between layers in **1** are weak, due to the separation by the quinolinium ions. The closest Br···Br contacts between layers are 5.742 Å with $\theta_1 = \theta_2 = 136.79°$ and $t = 0°$. These contacts are 13% larger than the corresponding contacts between layers in $(5MAP)_2CuBr_4$ [3] and $(5BAP)_2CuBr_4$[4] and 16% larger than observed in $(5CAP)_2CuBr_4$ (4.97 Å).[3] Thus a lower value for the ordering transition temperature T_N is expected. The upper limit for $|k_BT_N/2J|$ in **1** is ≤0.29, since susceptibility and high-field magnetization data suggest that T_N is below 1.8 K. This figure of merit is well below other 2D tetrabromocuprate systems, such as in $(5MAP)_2CuBr_4$ ($2J/k_B = -6.5(2)$ K, $|k_BT_N/2J| = 0.62$),[3] $(5BAP)_2CuBr_4$ ($2J/k_B = -6.94(6)$ K, $|k_BT_N/2J| = 0.58$),[3] and $(5CAP)_2CuBr_4$ ($2J/k_B = -8.5$ K, $|k_BT_N/2J| = 0.60$)[4] in agreement with the improved isolation of the layers by the large quinolinium ions.

The significance of the increased interlayer distance goes well beyond the simple increase of ≈15% of the closest Br···Br contacts. The 3D magnetic ordering temperature T_N is a function of the ratio of the interlayer to intralayer exchange constants, J'/J, with an order of magnitude decrease in the ratio leading to a reduction in T_N by roughly a factor of 3.[28] Using the $T_N/2|J| = 3.8$ K/6.5K = 0.58 value for $(5MAP)_2CuBr_4$ [3] yields $J'/J = 0.21$ based on the analysis of ref 28. For **1**, $T_N \leq 1.8$ K, $2|J| = 6.17$ K, and $T_N/2|J| \leq 0.29$, $J'/J \leq 4 \times 10^{-3}$, a reduction by more than a factor of 50. Such a major reduction is understandable given that the magnetic interaction pathway Cu−Br···Br−Cu depends on the overlap of the d-orbital wave functions transferred to the bromides; for widely separated bromide ions, the overlap decreases exponentially with the Br···Br distance so even an increase of 0.2 Å can be significant. Comparing the interlayer Br···Br distances of $(5MAP)_2CuBr_4$[3] to**1** shows an increase of more than 0.7 Å, consistent with the dramatic decrease in $T_N/2|J|$.

Careful examination of the structural parameters associated with the two-halide exchange pathway in both **1** and **2** provides insight into the magnetic-structural correlations of the two-halide exchange pathway between $CuBr_4^{2-}$ ions (see Table 4). Magneto-structural correlations in tetrabromocuprate compounds have revealed that exchange strengths have a strong dependence on the Br···Br distance.[17] On the sole basis of the Br···Br distances, the exchange strength between tetrahedra should be greater in **2** than in **1**, although the opposite is observed. This can be explained by examination of the angle parameters θ_1, θ_2, and τ, which are more favorable in **1** in comparison to **2**. For a two-halide exchange pathway, the exchange increases as θ_1 and θ_2 approach 180° and as τ approaches 0° or 180°. In linear cases, $\theta_1 = \theta_2 = 180°$ (in which case τ is undefined), the exchange has been reported as large as $2J/k_B = -234$ (1) K.[29] For **1**, the values for θ_1 and θ_2 are both larger than observed for the shorter contact in **2**, and τ (16.0°) in **1** is significantly closer to 0° than in **2** (53.5°). This appears to be sufficient to reduce the magnitude of the magnetic exchange in spite of the smaller Br···Br distance in **2**.

Given these results, it is clear that **1** represents the compound with the best combination of well-isolated 2D-square lattices and a small (17 T) saturation field reported to date. As such, it is an excellent candidate with which to examine the field-dependence of the energy spectrum of a 2D $S = {}^1/_2$ Heisenberg antiferromagnet.[30] Experiments to confirm the magnetic ordering temperature and synthesis of the perdeuterated material are in progress.

Acknowledgment. We are grateful for grants from the NSF (Grant IMR-0314773) toward purchase of the

(27) Xiao, F.; Woodward, F. M.; Landee, C. P.; Turnbull, M. M.; Mielke, C.; Harrison, N.; Lancaster, T.; Blundell, S. J.; Baker, P. J.; Babkevich, P.; Pratt, F. L. *Phys. Rev. B* **2009**, *79*, 134412.

(28) Yasuda, C.; Todo, S.; Hukushima, K.; Alet, F.; Keller, M.; Troyer, M.; Takayama, H. *Phys. Rev. Lett.* **2005**, *94*, 217201.

(29) Butcher, R. T.; Turnbull, M. M.; Landee, C. P.; Wells, B. M.; Novoa, J. J.; Ribas-Ariño, J.; Sandvik, A. W.; Awwadi, F. F. *Chem. Commun.* **2009**, 1359–61.

(30) Tsyrulin, N.; Pardini, T.; Singh, R. R. P.; Xiao, F.; Link, P.; Schneidewind, A.; Hiess, A.; Landee, C. P.; Turnbull, M. M.; Kenzelmann, M. *Phys. Rev. Lett.* **2009**, *102*, 197201.

MPMS SQUID, from PCISynthesis Inc. toward the purchase of the D8 powder X-ray diffractometer, and the Kresge Foundation toward the purchase of both. The authors thank Prof. Frederick T. Greenaway for assistance with the EPR spectroscopy. A portion of this work was performed at the National High Field Laboratory, which is supported by NSF Cooperative Agreement No. DMR-0084173 and by the state of Florida. The Bruker (Siemens) SMART APEX diffraction facility was established at the University of Idaho with the assistance of the NSF-EPSCoR program and the M. J. Murdock Charitable Trust, Vancouver, WA.

Supporting Information Available: Additional experimental details (CIF files). This material is available free of charge via the Internet at http://pubs.acs.org.